

# BIS(PYRIDYL) ANCILLARY LIGANDS AND PYRAZINE SULFONIC ACID IN THE SYNTHESIS OF TWO Ag(I) SUPRAMOLECULAR STRUCTURES AND FLUORESCENT PROPERTIES OF THE LATTER

Y.-J. Liang<sup>1</sup>, G. Feng<sup>2</sup>, X. Zhang<sup>1</sup>, J.-X. Li<sup>3\*</sup>,  
and Y. Jiang<sup>4\*\*</sup>

The coordination behavior of metal ions coordinated with heterocyclic sulfonic acid is of great significance for the construction of functional sulfonate polymers and the exploration of their potential application. In this study, two novel Ag(I)-based supramolecular structures, namely  $\{[\text{Ag}_2(4,4'\text{-bipy})_2][\text{Ag}_2(\text{P}-\text{SO}_3)_4]\cdot\text{H}_2\text{O}\}_n$  (**1**) and  $\{[\text{Ag}(\text{dpp})](\text{P}-\text{SO}_3)\cdot\text{H}_2\text{O}\}_n$  (**2**) ( $4,4'\text{-bipy}$  =  $4,4'\text{-bipyridine}$ , dpp = 1,3-di(4-pyridyl)propane, and  $\text{P}-\text{SO}_3\text{H}$  = pyrazine sulfonic acid) are synthesized using bis(pyridyl) ancillary ligands to assist the  $\text{P}-\text{SO}_3\text{H}$  main ligand by the solvent evaporation method. The single crystal X-ray diffraction data indicate that the as-synthesized polymers belong to  $P-1$  and  $P2_1/n$  space groups, respectively. In particular, the application of bis(pyridyl) ancillary ligands specifically improves the rigidity and coordination ability of pyrazine sulfonate, and then, it combines with the generated weak interaction to further extend the structure to higher dimensions. Powder X-ray diffraction results and related data, including Raman spectra, thermal stability and solid-state fluorescence characterizations, are also discussed.

**DOI:** 10.1134/S0022476621020153

**Keywords:** pyrazine sulfonate, silver polymer, weak interaction, crystal engineering, luminescent property.

## INTRODUCTION

Much attention has been paid to synthetic rules, structural evolution, and physicochemical properties of coordination polymers [1-10], especially nitrogen heterocyclic sulfonic acid-based coordination polymers [11-14]. By taking advantage of the flexible coordination mode of the sulfonic acid group, a high-dimensional framework can be formed by means of the bridging effect and it can act as an excellent hydrogen bond acceptor to conduct the construction of supramolecular structures [11-14]. Ag(I) sulfonates are the most representative sulfonate complexes that have been widely investigated. Numerous cases of novel structures with potential applications can be found in the literature [15-17].

---

<sup>1</sup>School of Medical Engineering, Foshan University, Foshan, People's Republic of China. <sup>2</sup>Jiangsu Cancer Hospital, Cancer Hospital of Nanjing Medical University, Nanjing, People's Republic of China. <sup>3</sup>Henan Key Laboratory of Function-Oriented Porous Materials, College of Chemistry and Chemical Engineering, Luoyang Normal University, Luoyang, People's Republic of China; \*ljx6281@126.com. <sup>4</sup>School of Chemistry and Chemical Pharmaceutical Science, Guangxi Normal University, Guilin, People's Republic of China; \*\*ymjiang@mailbox.gxnu.edu.cn. Original article submitted August 4, 2020; revised September 7, 2020; accepted September 8, 2020.

Notably, Ag(I) is capable of producing stable and spatially diverse structures in terms of  $M\cdots M$ ,  $M\cdots C$ ,  $X-H\cdots M$ , or  $M\cdots \pi$  interactions during the coordination process, and crystallographically characterized Ag(I) complexes with coordination numbers from two to eight have been reported [18, 19]. For instance, Brenna et al. [20] synthesized an Ag(I) coordination polymer with 3,5-dimethyl-4-sulfonated pyrazole and found that the SO<sub>3</sub>Na substituent in the pyrazole ring can lead to a three dimensional (3D) polymeric species interconnected through the bridging effect. In particular, the unique trapezoidal grid, which comprises Na<sup>+</sup> ions and interconnected bridging sulfonates, may lead to the slow reorganization of disordered moieties in a time-controlled crystallization process. Just recently, Almeida et al. [21] prepared a water-soluble one-dimensional (1D) Ag(I) tris(pyrazolyl) methane sulfonate polymer and proved that the novel structure features a high antiproliferative activity, which could be a suitable cancer therapy as it induces apoptosis. Nevertheless, the study of metal ions coordinated with N-containing heterocyclic sulfonates remains insufficient, and little information can be found regarding the use of pyrazine sulfonic acid as the main ligand to construct functional polymers. In addition, the synthesis, properties, and further applications of such compounds remain a challenge. From our previous study, the 1D Ag(I) coordination polymer with pyrazine sulfonic acid has a potential for application in optical sensing [22]. We speculate that more valuable silver sulfonate supramolecular structures with potential applications can be produced through rational design [23-25]. For this purpose, bis(pyridyl) ligands were introduced along with pyrazine sulfonic acid (P-SO<sub>3</sub>H) to assist the assembly of Ag(I) polymers. Two novel Ag(I) supramolecular structures {[Ag<sub>2</sub>(4,4'-bipy)<sub>2</sub>][Ag<sub>2</sub>(P-SO<sub>3</sub>)<sub>4</sub>]·H<sub>2</sub>O}<sub>n</sub> (**1**) and {[Ag(dpp)](P-SO<sub>3</sub>)·H<sub>2</sub>O}<sub>n</sub> (**2**) (4,4'-bipy = 4,4'-bipyridine, dpp = 1,3-di(4-pyridyl)propane) were obtained, in which the main P-SO<sub>3</sub> ligand acts as an anionic ligand and an uncoordinated counterbalancing anion. The crystal structures and related properties are discussed in detail. This study will help provide new insights for exploring the functional pyrazine sulfonated supramolecular assembly.

## EXPERIMENTAL

### Materials and methods

All reagents were of analytical grade and used without further purification. The pyrazine sulfonic acid ligand (P-SO<sub>3</sub>H) was prepared following the previous report [26].

**Preparation of {[Ag<sub>2</sub>(4,4'-bipy)<sub>2</sub>][Ag<sub>2</sub>(P-SO<sub>3</sub>)<sub>4</sub>]·H<sub>2</sub>O}<sub>n</sub> (**1**)**. Typically, AgSCN (0.4 mmol) and pyrazine sulfonic acid (P-SO<sub>3</sub>H), (0.3 mmol) were mixed with solvents (acetone and acetonitrile in a certain proportion of 1:3). Subsequently, an aqueous solution of 4,4'-bipy (0.3 mmol) was added to the mixture, which was then kept in the dark and stirred at 50 °C for 6 h. The filtrate was allowed to naturally evaporate at room temperature to afford a needle-like crystal after 55 days. The yield was 23% (based on Ag). The calculated values (%) for C<sub>36</sub>H<sub>30</sub>N<sub>12</sub>S<sub>4</sub>Ag<sub>4</sub>O<sub>13</sub> were C 30.92, H 2.16, and N 12.02. The actual values were as follows: C 30.74, H 1.95, and N 11.84. The infrared data were as follows (KBr, cm<sup>-1</sup>): 3472 s, 2423 w, 1643 s, 1599 m, 1385 vs, 1228 vs, 1061 m, 1037 m, 1071 vs, 1037 vs, 810 m, and 654 s.

**Preparation of {[Ag(dpp)](P-SO<sub>3</sub>)·H<sub>2</sub>O}<sub>n</sub> (**2**)**. The synthetic process of **2** was similar to that of **1**, except the precursor was replaced with Ag<sub>2</sub>MoO<sub>4</sub> and the second ligand was changed to dpp. The yield was 19% (based on Ag). The calculated values (%) for C<sub>17</sub>H<sub>19</sub>N<sub>4</sub>SAgO<sub>4</sub> were C 42.25, H 3.95, and N 11.59. The actual values were C 42.75, H 4.23, and N 11.89. The infrared data were as follows (KBr, cm<sup>-1</sup>): 3484 m, 3356 m, 1664 s, 1386 vs, 1217 vs, 1053 vs, 1039 vs, 863 m, 650 vs, 531 s, and 436 m.

**X-ray crystallography.** The diffraction data on **1** and **2** were collected on an Agilent Super-Nova diffractometer (MoK<sub>α</sub>,  $\lambda = 0.071073$  nm) and handled with the Olex2 software [27]. The full matrix least squares method in the SHELXTL program package was used to solve and refine the structure. Moreover, anisotropic thermal parameters were applied to all non-hydrogen atoms [28]. Crystallographic data, selected bond distances and angles of **1** and **2** are presented in Tables 1 and 2, respectively; the hydrogen bonds are listed in Table 3.

**TABLE 1.** Crystal Data and Structure Refinement for **1** and **2**

Parameter	<b>1</b>	<b>2</b>
Empirical formula	C <sub>36</sub> H <sub>30</sub> N <sub>12</sub> S <sub>4</sub> Ag <sub>4</sub> O <sub>13</sub>	C <sub>17</sub> H <sub>19</sub> N <sub>4</sub> SAgO <sub>4</sub>
Formula weight	1398.43	483.29
Crystal system	Triclinic	Monoclinic
Space group	P-1	P2 <sub>1</sub> /n
<i>a</i> , <i>b</i> , <i>c</i> , Å	11.3851(3), 13.5140(8), 14.5767(6)	10.1057(7), 8.9885(3), 21.2214(10)
α, β, γ, deg	74.044(5), 89.772(3), 88.950(3)	90.00, 98.617(6), 90.00
<i>V</i> , Å <sup>3</sup>	2155.98(17)	1905.90(17)
<i>Z</i>	2	4
Absorption coefficient, mm <sup>-1</sup>		
<i>F</i> (000)	2.063	1.195
θ, deg	1313	901
Reflections collected	2.90 to 26.37	2.98 to 26.37
Unique data	53239	8115
<i>R</i> <sub>int</sub>	8811	3901
Completeness to θ, %	0.0672	0.0240
Data / restraints / parameters	99.9	99.9
<i>GOOF</i> on <i>F</i> <sup>2</sup>	8811 / 3 / 628	3901 / 3 / 250
Final <i>R</i> indices ( <i>I</i> > 2σ( <i>I</i> ))	1.161	1.033
<i>R</i> indices (all data)	<i>R</i> <sub>1</sub> = 0.1140, <i>wR</i> <sub>2</sub> = 0.2984	<i>R</i> <sub>1</sub> = 0.0324, <i>wR</i> <sub>2</sub> = 0.0639
Largest diff. peak / hole, e/Å <sup>3</sup>	<i>R</i> <sub>1</sub> = 0.1292, <i>wR</i> <sub>2</sub> = 0.3063	<i>R</i> <sub>1</sub> = 0.0436, <i>wR</i> <sub>2</sub> = 0.0709
	4.126 / -1.613	0.282 / -0.465

**TABLE 2.** Selected Bond Distances (Å) and Bond Angles (deg) for **1** and **2**

<b>1</b>		<b>2</b>	
Bond distance			
Ag1—N5	2.202(12)	Ag1—N1	2.145(2)
Ag1—N1	2.255(12)	Ag1—N2 <sup>#4</sup>	2.148(2)
Ag1—N3	2.469(12)	Ag1—Ag1 <sup>#5</sup>	3.0245(5)
Ag3—N9	2.149(13)	Ag1—N2 <sup>#6</sup>	2.148(2)
Ag4—N11	2.141(12)	N1—Ag1—N2 <sup>#4</sup>	164.67(8)
Ag4—N12 <sup>#2</sup>	2.173(12)	C1—N1—Ag1	120.2(17)
Bond angle			
N5—Ag1—N1	163.2(5)	C5—N1—Ag1	122.9(18)
N5—Ag1—N3	101.0(4)	C12—N2—Ag1 <sup>#6</sup>	121.6(18)
N1—Ag1—N3	95.0(4)	N1—Ag1—Ag1 <sup>#5</sup>	87.97(6)
N7—Ag2—N6	93.8(4)	N2 <sup>#4</sup> —Ag1—Ag1 <sup>#5</sup>	100.49(6)
N4 <sup>#1</sup> —Ag2—N6	104.7(4)	N10 <sup>#4</sup> —Ag3—N9	176.8(6)

Symmetry transformations used to generate equivalent atoms: <sup>#1</sup> *x*−1, *y*, *z*; <sup>#2</sup> *x*+1, *y*, *z*; <sup>#4</sup> *x*+1/2, *−y*+1/2, *z*−1/2; <sup>#5</sup> *x*−2, *−y*, *−z*+1; <sup>#6</sup> *x*−1/2, *−y*+1/2, *z*+1/2.

## RESULTS AND DISCUSSION

### Structural description

**Structural description of {[Ag<sub>2</sub>(4,4'-bipy)<sub>2</sub>]<sup>+</sup>[Ag<sub>2</sub>(P-SO<sub>3</sub>)<sub>4</sub>]·H<sub>2</sub>O<sub>n</sub>}** (**1**). The crystallographic results showed that Ag<sup>+</sup> ions adopt two coordination modes when bonded to a sulfonate ligand and a 4,4'-bipy molecule (Fig. 1*a*). The [Ag<sub>2</sub>(4,4'-bipy)<sub>2</sub>]<sup>+</sup> composition is regarded as the counterocation that constructs 1D double chains in the equatorial direction. The

**TABLE 3.** Hydrogen Bond Geometries ( $\text{\AA}$ , deg) for **1** and **2**

$D-\text{H}\cdots A$	$d(D-\text{H})$	$d(\text{H}\cdots A)$	$d(D\cdots A)$	$\angle(D\text{H}A)$
Compound <b>1</b>				
O13–H13A…O1 <sup>#3</sup>	0.84	2.25	2.73(7)	117
O13–H13B…O4	0.85	2.00	2.69(5)	137
Compound <b>2</b>				
O4–H4A…O3 <sup>#7</sup>	0.85	2.51	2.51(4)	175
O4–H4B…O3 <sup>#8</sup>	0.85	2.38	2.38(3)	122

Symmetry code: <sup>#3</sup>  $-x+1, -y+2, -z$ ; <sup>#7</sup>  $-x+3/2, y+1/2, -z+1/2$ ; <sup>#8</sup>  $x, y+1, z$ .

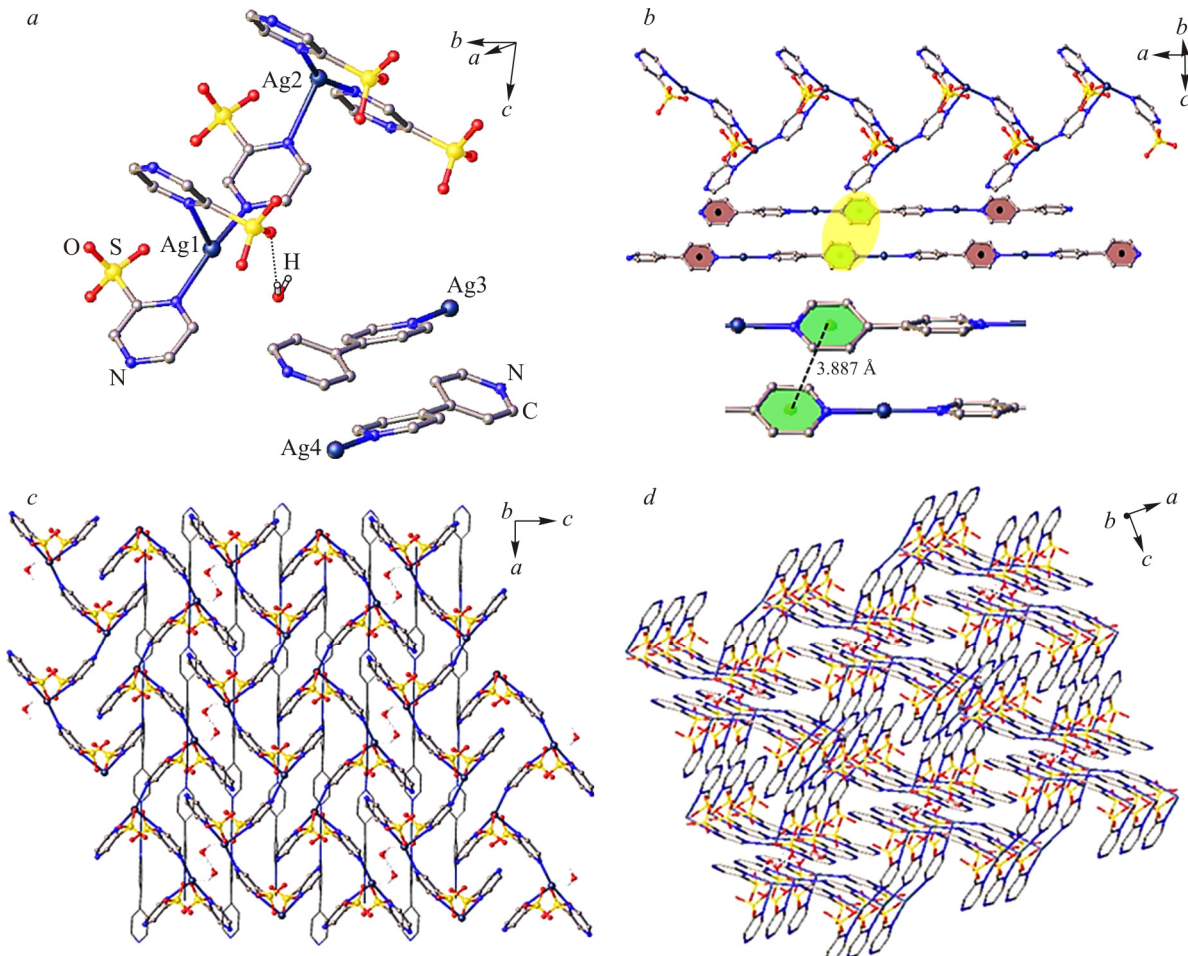


**Fig. 1.** Coordination environments of Ag(I) ions in  $\{[\text{Ag}_2(4,4'\text{-bipy})_2][\text{Ag}_2(\text{P-SO}_3)_4]\cdot\text{H}_2\text{O}\}_n$  (**1**) (*a*); the one-dimensional structure and the distance of the pyrazine ring in the double chain in **1** (*b*); the 2D crystal network of **1** (*c*); 3D structure of **1** constructed through  $\pi-\pi$  and hydrogen bond interactions (*d*).

centroid-to-centroid distance in the pyridine ring was detected to be 3.88  $\text{\AA}$  (Fig. 1*b*). In particular, a three-chain stabilization module was formed, which turned into a two-dimensional (2D) network through the counterocation and the counteranion combination formulated as  $[\text{Ag}_2(\text{P-SO}_3)_4]$ . The two contact angles including the sulfonate anions were measured as  $101^\circ$  and  $93.79^\circ$  for N5–Ag1–N3 and N6–Ag2–N7, respectively, which is consistent with the previous studies (Fig. 1*c*) [29]. Moreover, free water molecules were involved in a large number of hydrogen bonds. They and the rich weak stacking interaction between counterions are responsible for the construction of a 3D supramolecular structure (Fig. 1*d*).

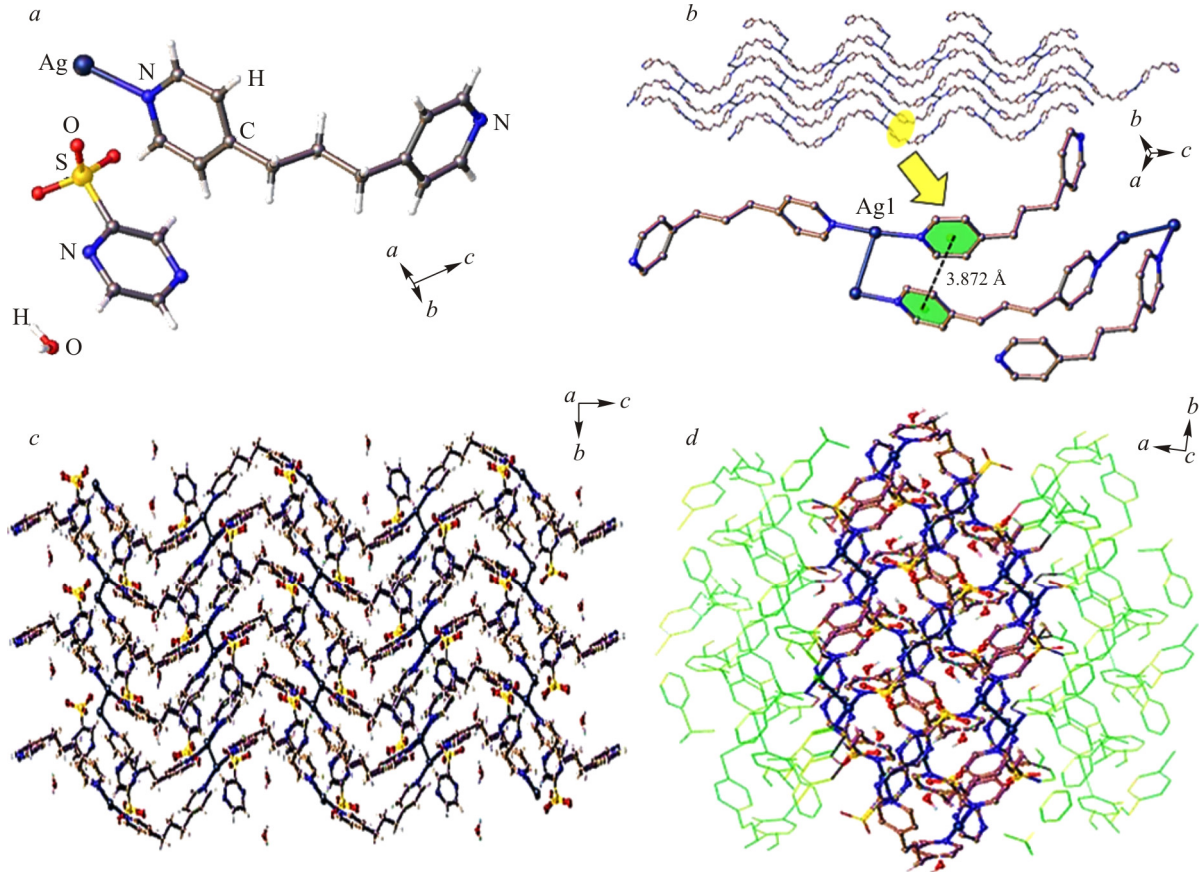


**Fig. 2.** Coordination environments of the Ag(I) ion in  $\{[Ag(dpp)](P-SO_3)\cdot H_2O\}_n$  (**2**) (*a*); 1D structure and the centroid-to-centroid distance between the pyrazine rings in **2** (*b*); 2D crystal network of **2** (*c*); 3D structure of **2** constructed via  $\pi-\pi$  and hydrogen bond interactions (*d*).

**Structural description of  $\{[Ag(dpp)](P-SO_3)\cdot H_2O\}_n$  (**2**).** The coordination environment in **2** contains only one crystallographically independent  $Ag^+$  ion, and the asymmetric unit comprises a cationic complex  $[Ag(dpp)]^+$  and the  $P-SO_3$  counteranion together with one water molecule (Fig. 2*a*). The  $Ag^+$  ion first combines with the pyridine nitrogen atom in the dpp ligand in a bridging coordination mode to construct a 1D chain, which then extends into a 2D wave-like network through the argentophilic bonding  $Ag1-Ag1^{#5}$  (3.024 Å). The centroid-to-centroid distance between the pyridine rings was 3.87 Å, and this value, as well as the  $Ag-Ag$  bond distance, is consistent with those of the other related silver polymers (Fig. 2*b, c*) [30]. Unlike 4,4'-bipy, the dpp ligand is more flexible and can be tuned and modified for the construction of strong structures that are assembled in a stacking manner [31]. Therefore, the construction of a 3D supramolecular structure can be achieved through the hydrogen bonding induced by the introduction of free solvent molecules and the stacking interaction between nitrogen-containing heterocycles (Fig. 2*d*).

#### Powder X-ray diffraction

The results of powder X-ray diffraction (PXRD) indicated that all peaks in the experimental patterns matched with those in the simulated patterns, indicating the phase purity for the bulk phases of **1** and **2**, respectively (Fig. 3).

#### Thermal analysis

The thermogravimetric measurement of **1** and **2** was performed between room temperature and 800 °C with a heating rate of 10 °C/min under an  $N_2$  flow. As shown in Fig. 4, **1** first, there is a gradual weight loss from room temperature to approximately 92 °C for **1**, which is assigned to the loss of water (observed 8.7%, calculated 7.3%). The next inflection

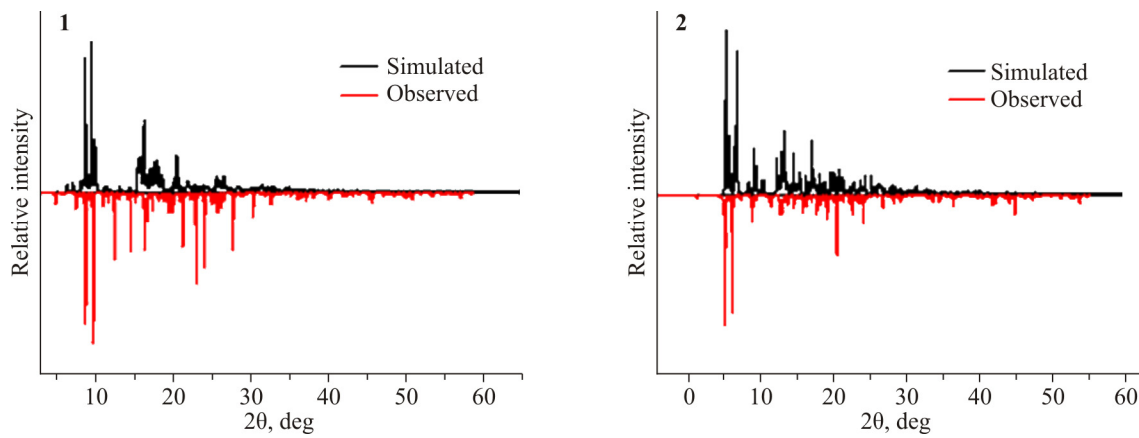


**Fig. 3.** PXRD of  $\{[Ag_2(4,4'-bipy)_2][Ag_2(P-SO_3)_4]\cdot H_2O\}_n$  (**1**) and  $\{[Ag(dpp)](P-SO_3)\cdot H_2O\}_n$  (**2**) at room temperature.

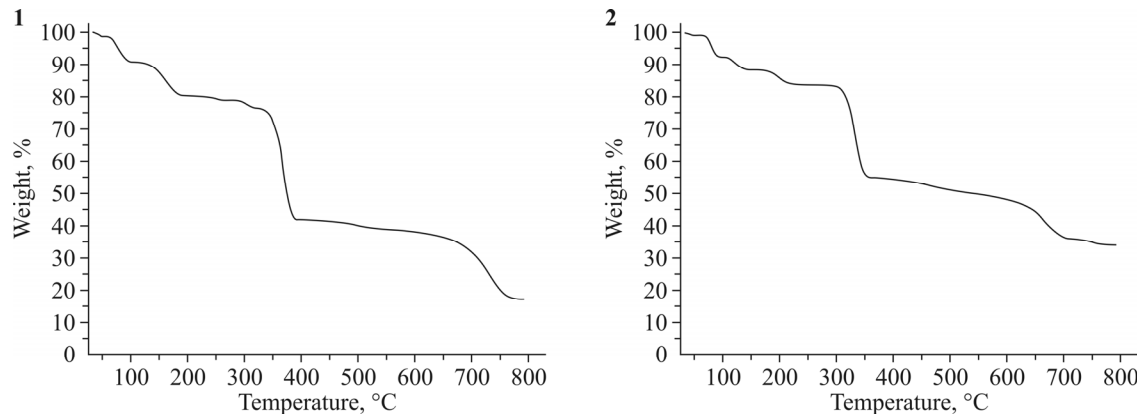


**Fig. 4.** TGA curves of  $\{[Ag_2(4,4'-bipy)_2][Ag_2(P-SO_3)_4]\cdot H_2O\}_n$  (**1**, *a*) and  $\{[Ag(dpp)](P-SO_3)\cdot H_2O\}_n$  (**2**, *b*) in the solid state.

point appeared as the temperature increased to 180 °C (observed 10.1%, calculated 8.7%). In particular, rapid decomposition with the maximum weight loss occurred at 335 °C. The degradation rate decreased until the formation of Ag<sub>2</sub>O at approximately 800 °C (observed 17.4%, calculated 15.2%). For **2**, the thermal decomposition trend was similar to that of **1**, except the release of guest molecules was observed until approximately 103 °C (observed 7.4%, calculated 7.1%), and the maximum weight loss appeared at approximately 294 °C, which was assigned to the rapid decomposition of the framework. Finally, at approximately 800 °C the Ag<sub>2</sub>O residue formed (observed 33.2%, calculated 31.9%) (Fig. 4, **2**).

#### Raman characterization

The solid-state Raman signals of **1** and **2** under different pH conditions can be seen in Fig. 5. For **1**, the peaks at approximately 700 cm<sup>-1</sup> were assigned to the S=O bending vibration in the P-SO<sub>3</sub> ligand. Furthermore, the signal between 300 cm<sup>-1</sup> and 400 cm<sup>-1</sup> was attributed to Ag–O and Ag–N asymmetric vibrations. Notably, the bending vibration of the sulfonate ligand became weaker as the pH value decreased. However, the Ag–O and Ag–N vibration was hardly affected, and the intensity of the Raman signal for the asymmetric vibration of Ag–O and Ag–N decreased as the pH value increased, especially at the pH value of 11 (Fig. 5, **1**). Moreover, the Raman signals of **2** under different pH conditions were similar to those of **1**, except a splitting peak at approximately 300 nm at pH = 3, which may be attributed to the stretching vibration of Ag–N in the dpp ligand (Fig. 5, **2**). To the best of our knowledge, Raman features suggest the defect, crystallinity, and character of the as-synthesized crystal structure to some extent. Hence, we suppose that the variation in the Ag bonding signals are induced by different proton interactions through different pH conditions [32, 33].

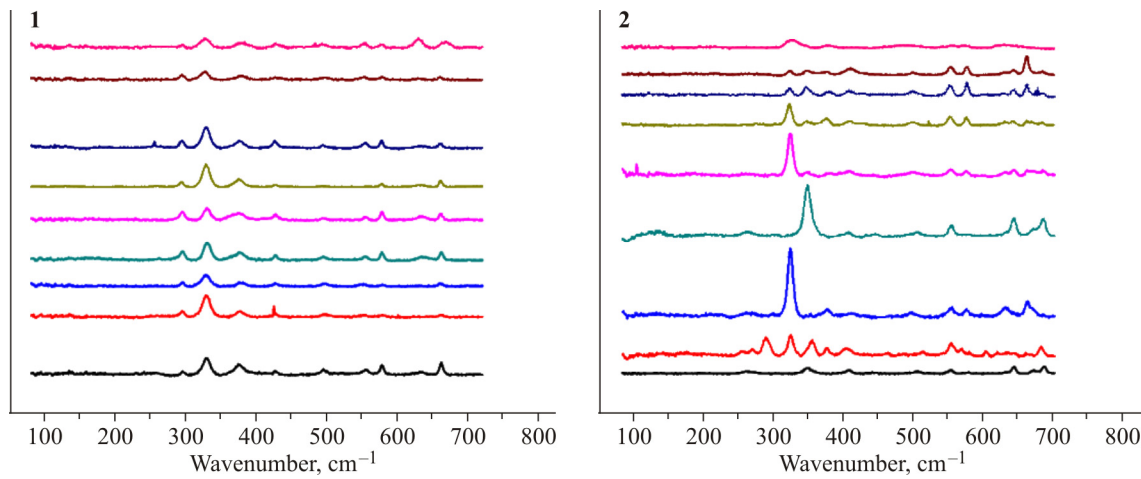


**Fig. 5.** Raman spectra of  $\{[\text{Ag}_2(4,4'\text{-bipy})_2][\text{Ag}_2(\text{P-SO}_3)_4]\cdot\text{H}_2\text{O}\}_n$  (**1**) and  $\{[\text{Ag}(\text{dpp})](\text{P-SO}_3)\cdot\text{H}_2\text{O}\}_n$  (**2**) under different pH conditions: 3, 4, 5, 6, 8, 9, 10, 11 down up.

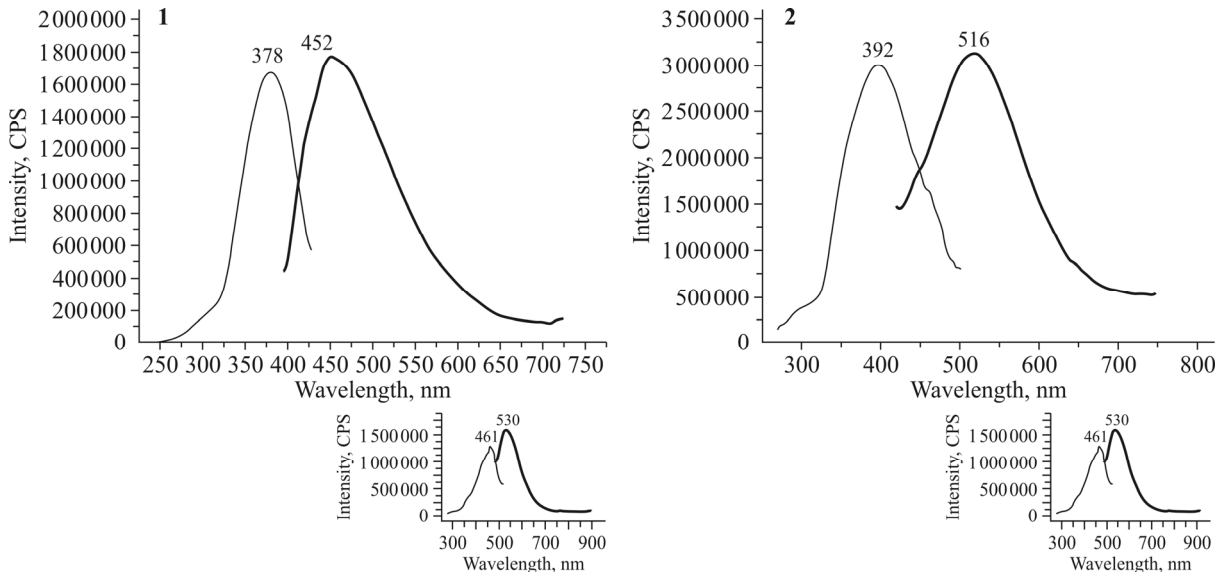


**Fig. 6.** Photoluminescence spectra of **1**  $\{[\text{Ag}_2(4,4'\text{-bipy})_2][\text{Ag}_2(\text{P-SO}_3)_4]\cdot\text{H}_2\text{O}\}_n$  and **2**  $\{[\text{Ag}(\text{dpp})](\text{P-SO}_3)\cdot\text{H}_2\text{O}\}_n$  in the solid state (insets show the spectra for the respective ligand).

### Fluorescent properties

The solid-state luminescent properties of **1** and **2** were measured at room temperature. The maximum emission of **1** was detected at 452 nm at excitation of 378 nm; the fluorescence intensity was much stronger than that of the ligand ( $\lambda_{\text{ex}} = 461$  nm and  $\lambda_{\text{em}} = 530$  nm) with the emission position undergoing a blue shift of 78 nm (Fig. 6, **1**). An increase in the intensity may arise from 4,4'-bipy participating in the coordination of **1**, forming a highly conjugated electron conducting system through the  $\pi$  to  $\pi^*$  electron transition, thus promoting luminescence and energy transfer [34]. In turn, the fluorescence intensity of **2** ( $\lambda_{\text{ex}} = 392$  nm and  $\lambda_{\text{em}} = 516$  nm) was much stronger than that of **1** and exhibited a blue shift of 14 nm when compared to the P-SO<sub>3</sub> ligand. The dpp ligand acts as a long chain electron bridge supporting the ligand-to-metal and metal-to-ligand electron transfer modes and inhibits proton conduction, which results in a significant increase in the fluorescence intensity (Fig. 6, **2**) [35].

## CONCLUSIONS

In this study, two sulfonate-based silver polymers were fabricated using pyrazine sulfonate and bis(pyridyl) ancillary ligands. The crystal structures and related data, including PXRD, Raman spectroscopy, thermal stability, and solid-state fluorescence were discussed. The employment of bis(pyridyl) ancillary ligands effectively improved the rigidity of the pyrazine sulfonate linking during the coordination process, thereby assisting the formation of high-dimensional structures. The supramolecular structures of as-synthesized Ag(I) polymers are a result of the combined action of the stacking interaction between N-containing heterocyclic rings and the generation of hydrogen bonds in free solvent molecules. Further studies with in vitro cell experiment are in progress.

## FUNDING

The research was supported by the Key scientific research projects in Colleges and Universities of Henan province (No. 17A150040) and the Scientific Research Program of High-Level Talents of Foshan University (CGG07118).

## ADDITIONAL INFORMATION

Author contributions. Yi-Jun Liang: design and performance of the experiments, manuscript written. Guodong Feng and Xiaoli Zhang: data analysis and discussion of the results. Jun-Xia Li and Yimin Jiang: supervision and revision of the manuscript. All authors have given approval to the final version of the manuscript.

Crystallographic data of the structural analysis have been deposited with the Cambridge Crystallographic Data Center (CCDC deposition numbers 1999968 (1) and 1999969 (2)). Copies of this information may be obtained free of charge from CCDC, 12 Union Road, Cambridge, CB2 1EZ, UK (Fax: þ44 1223 336 033; e-mail: deposit@ccdc.cam.ac.uk or www.ccdc.cam.ac.uk).

## CONFLICT OF INTERESTS

The authors declare that they have no conflict of interests.

## REFERENCES

1. Z. Zheng, P. Xu, Y. Jiang, Y.-J. Liang, and J.-X. Li. *J. Struct. Chem.*, **2021**, *62*, 308.
2. J. X. Li, Z. X. Du, L. Y. Xiong, L. L. Fu, and W. B. Bo. *J. Solid State Chem.*, **2021**, *293*, 121799.
3. J. X. Li, Z. X. Du, L. L. Zhang, D. L. Liu, and Q. Y. Pan. *Inorg. Chim. Acta*, **2020**, *512*, 119890.
4. J. X. Li, Z. X. Du, Q. Y. Pan, L. L. Zhang, and D. L. Liu. *Inorg. Chim. Acta*, **2020**, *509*, 119677.
5. Z. X. Du, J. X. Li, S. J. Liu, Z. Q. Wang, and Q. J. Pan. *Z. Naturforsch.* **2020**, *75(6-7)b*, 567.
6. J. X. Li and Z. X. Du. *J. Coord. Chem.*, **2016**, *69*, 2563.
7. J. X. Li, Z. X. Du, J. Wang, and X. Feng. *Z. Naturforsch.* **2019**, *74(11–12)b*, 839.
8. J. X. Li, Z. X. Du, and X. Feng. *Z. Naturforsch.* **2019**, *74(11–12)b*, 833..
9. J. X. Li and Z. X. Du. *J. Clust. Sci.*, **2020**, *31*, 507.
10. Z. X. Du and J. X. Li. *Z. Naturforsch.*, **2020**, *75b(6–7)*, 577.
11. D. K. Maity, S. Ghosh, K. Otake, H. Kitagawa, and D. Ghoshal. *Inorg. Chem.*, **2019**, *58*, 12943.
12. M. M. Islam, P. Bhanja, M. Halder, A. Das, A. Bhaumik, and I. Sk. Manirul. *Mol. Catal.*, **2019**, *475*, 110489.
13. C. Kahrs, M. Schmidtmann, M. S. Wickleder, and J. Christoffers. *Eur. J. Inorg. Chem.*, **2018**, *46*, 6499.
14. O. Beyer, T. Homburg, M. Albat, N. Stock, and U. Lüning. *New J. Chem.*, **2017**, *41*, 8870.
15. X. L. Zhang, G. M. Tang, and Y. T. Wang. *Polyhedron*, **2018**, *148*, 55.

16. Y. Meng, Y. Ruan, J. Mo, B. L. Liu, A. Y. Wan, and H. P. Xiao. *Transition Met. Chem.*, **2017**, *42*, 285.
17. E. Soe, J. S. Kim, I. Chakraborty, and S. R. J. Oliver. *Eur. J. Inorg. Chem.*, **2019**, 2175.
18. D. Davarci, R. Gür, S. Besli, E. Senkuytu, and Y. Zorlu. *Acta Crystallogr.*, **2016**, *B72*, 344.
19. A. G. Young and L. R. Hanton. *Coord. Chem. Rev.*, **2008**, *252*, 1346.
20. S. Brenna, G. A. Ardizzoia, V. Colombo, and A. Sironi. *CrystEngComm*, **2019**, *21*, 4586.
21. J. Almeida, C. Roma-Rodrigues, A. G. Mahmoud, M. F. C. Guedes da Silva, A. J. L. Pombeiro, L. M. D. R. S. Martins, P. V. Baptista, and A. R. Fernandes. *J. Inorg. Biochem.*, **2019**, *199*, 110789.
22. Y. Liang, X. Meng, F. Huang, J. J. Guo, and Y. M. Jiang. *J. Coord. Chem.*, **2011**, *64*, 3751.
23. Z. X. Liu. *Synth. React. Inorg. Met.-Org., Nano-Met. Chem.*, **2016**, *46*, 809.
24. X. L. Zhang, G. M. Tang and Y. T. Wang. *Polyhedron*, **2018**, *147*, 26.
25. A. Tăbăcaru, C. Pettinari, M. Bușilă, and R. M. Dinică. *Polymers*, **2019**, *11*, 1686.
26. E. Hort and P. E. Spoerri. *J. Am. Chem. Soc.*, **1948**, *70*, 1657.
27. O. V. Dolomanov, L. J. Bourhis, R. J. Gildea, J. A. K. Howard, and H. Puschmann. *J. Appl. Crystallogr.*, **2009**, *42*, 339.
28. G. M. Sheldrick. SHELXS-97: Program for crystal structure solution, **1997**.
29. S. Welsch, C. Lescop, M. Scheer, and R. Reau. *Inorg. Chem.*, **2008**, *47*, 8592.
30. G. P. Yang, Y. Y. Wang, P. Liu, A. Y. Fu, Y. N. Zhang, J. C. Jin, and Q. Z. Shi. *Cryst. Growth Des.*, **2010**, *10*, 1443.
31. L. Carlucci, G. Ciani, D. W. Gudenberg, and D. M. Proserpio. *Inorg. Chem.*, **1997**, *36*, 3812.
32. A. P. Côté, M. J. Ferguson, K. A. Khan, G. D. Enright, A. D. Kulynych, S. A. Dalrymple, and G. K. H. Shimizu. *Inorg. Chem.*, **2002**, *41*, 287.
33. M. A. Omary, T. R. Webb, Z. Assefa, G. E. Shankle, and H. H. Patterson. *Inorg. Chem.*, **1998**, *37*, 1380.
34. S. Iyoshi and M. Taki, Y. Yamamoto. *Inorg. Chem.*, **2008**, *47*, 3946.
35. E. Wong, J. Li, C. Seward, and S. Wang. *Dalton Trans.*, **2009**, *10*, 1776.